Can We Merge *GEOSAT Follow-On* with TOPEX/Poseidon and *ERS-2* for an Improved Description of the Ocean Circulation?

P. Y. LE TRAON, Y. FAUGÈRE, F. HERNANDEZ, J. DORANDEU, F. MERTZ, AND M. ABLAIN

CLS Space Oceanography Division, Ramonville, France

(Manuscript received 18 April 2002, in final form 18 November 2002)

ABSTRACT

Merging *Geosat Follow-On* (*GFO*) with TOPEX/Poseidon (TP) and *ERS-2* altimeter data has the potential to improve the mapping of sea level and ocean circulation variations. This can be achieved, however, only if measurement errors and inconsistencies between the different missions are sufficiently reduced. In this paper, it is shown how to get consistent sea surface heights from the three missions using the most precise mission (TP) as a reference. A new technique is then used to estimate a *GFO* mean profile. This allows consistent sea level anomalies (SLAs) to be extracted from *GFO*, TP, and *ERS-2*. SLA data are then merged with a mapping technique that takes into account noise and residual long wavelength errors. Thanks to these techniques, it is shown that *GFO* can be combined with TP and *ERS-2* and that the combination provides a significant improvement in the description of the mesoscale circulation.

1. Introduction

Satellite altimetry has made a unique contribution to the observation and understanding of the global ocean circulation both at large scale and at the mesoscale (see Fu and Chelton 2001; Le Traon and Morrow 2001; Picaut and Busalacchi 2001, for a recent review). The surface dynamic topography as measured by satellite altimetry also provides a strong constraint to estimate and forecast the three-dimensional ocean state through data assimilation. Satellite altimetry is thus considered as one of the most important input datasets of the forthcoming Global Ocean Data Assimilation Experiment (GODAE) and its envisioned scientific and operational applications (International GODAE Steering Team 2001).

The main requirement for satellite altimetry is that at least two altimeter missions are needed with one being a very precise long-term altimeter system (e.g., Koblinsky et al. 1992). The long-term altimeter system is supposed to provide the large-scale climatic signals, while the combined data of several altimeters is needed to resolve the mesoscale ocean circulation. Since 1992, this minimum requirement has been fulfilled by the U.S./French TOPEX/Poseidon (TP) and the European Space Agency *ERS-1/2* missions. This time series is now extended with *Jason-1* and ENVISAT, the successors of TP and *ERS-1/2*. TOPEX/Poseidon has now been measuring the ocean topography with an unprecedented accuracy for more than 10 yr, while *ERS-1* and *ERS-2* have provided a very useful complementary sampling. The merging of TP and *ERS-1/2* has allowed, in particular, observation of the mesoscale variability with a resolution never before achieved (Ducet et al. 2000).

The U.S. Navy *Geosat Follow-On* (*GFO*) satellite was launched in February 1998 and was formally accepted by the navy on 29 November 2000. Its data are now available to the scientific community. This is a unique opportunity to characterize the signals missed by the merging of TP and ERS and to analyze the contribution of a third satellite for the mapping of mesoscale ocean variability. Several theoretical studies have shown that merging TP and *ERS-2* with *GFO* data should improve the mesoscale variability mapping (e.g., Jacobs et al. 2001; Le Traon et al. 2001). Merging of multiple altimeter datasets is, however, a difficult task. The altimeter sea surface heights (SSHs) measurements have biases and errors that can be very different among missions. These biases and errors must be reduced to get consistent and intercalibrated SSH data. Since geoids are not known with a sufficient accuracy, data along each satellite track need to be referenced to a mean profile (repeat-track analysis) to get sea level anomaly (SLA) measurements. Care should be taken to have consistent mean profiles for the different missions. This poses a specific and difficult problem for *GFO*.

In this article, we report on our first attempts to merge *GFO* with TP and *ERS-2* data. The paper is organized as follows. Section 2 deals with the merging methodology. We explain first how to get consistent SSH and

Corresponding author address: Dr. Pierre-Yves Le Traon, CLS Space Oceanography Division, 8-10 rue Hermès, Parc Technologique du Canal, Ramonville, St. Agne 31526, France.
E-mail: letraon@cls.fr

TABLE 1. Rms of crossover differences (cm) for *GFO*, *ERS-2*, and TP over the period 29 Nov 2000–15 Jan 2001. Only crossovers with a time difference below 10 days, in depths deeper than 200 m, and in areas with eddy variability below 20 cm rms are kept to minimize the effect of ocean variability.

Rms of crossover differences	TP/TP	*GFO/GFO*	TP/*GFO*	*ERS-2/ERS-2*	TP/*ERS-2*
Before adjustment	6.23	15.19	14.75	11.93	10.08
After adjustment	/	6.47	6.72	7.28	6.98

SLA data from the three altimeter missions. The mapping technique used to merge SLA data from *GFO*, TP, and *ERS-2* is then described. Results are presented in section 3. *GFO* data are first compared and then merged to TP and *ERS-2* data and we analyze the contribution of the merging. Main conclusions and perspectives are given in the final section.

2. Merging *GFO* data with TP and *ERS-2* data

a. Data

We used about 10 weeks of *GFO*, TP, and *ERS-2* data spanning the period from end of November 2000 to end of January 2001. This includes four *GFO* cycles (17-day repeat cycle), seven TP cycles (10-day repeat period), and two *ERS-2* cycles (35-day repeat cycle). TOPEX/Poseidon data are the M-GDR distributed by AVISO. The M-GDR tidal correction was replaced, however, by the more recent Goddard Ocean Tide (GOT99) tidal correction (Ray 1999) and we used an inverse barometer correction with a variable mean pressure. The near-real-time *GFO* MOE product distributed by the National Oceanic and Atmospheric Administration (NOAA) was used. *ERS-2* data are the near-real-time ESA Fast Delivery Product (FDP). Orbits are the DEOS fast-delivery *ERS-2* orbits (Scharroo and Visser 1998). Note that using the near-real-time *ERS-2* and *GFO* orbit significantly increases the initial orbit errors; however, as previously shown (e.g., Le Traon and Ogor 1998), the orbit error reduction method (see section 2b) is rather insensitive to the initial orbit used. When necessary, *ERS-2* and *GFO* altimetric corrections were updated to make the TP, *ERS-2*, and *GFO* corrections homogeneous. This holds for the tidal and inverse barometer corrections. We also used the Bent model to correct both *ERS-2* and *GFO* data for ionospheric error (TP is a dual-frequency altimeter and the ionospheric correction can be precisely derived from the combination of the two frequency range measurements).

TABLE 2. Rms (cm) of GFO − GFO ($G_{MP} - G_{MP}$), TP − GFO ($TP_{MP} - G_{MP}$), and ERS − GFO ($E_{MP} - G_{MP}$) mean profile crossover differences.

Mean profile (MP) crossover differences	$G_{MP} - G_{MP}$	$TP_{MP} - G_{MP}$	$E_{MP} - G_{MP}$
Raw *GFO* MP	8.46	8.01*	8.28*
GFO MP after adjustment onto TP and ERS MPs	2.99	4.05	4.02
Same as above plus an additional correction of medium scale differences	2.99	2.37	2.62

* After correcting *GFO* MP for a relative bias of 16 cm to make it consistent with TP.

b. GFO *orbit error reduction using TP as a reference*

Merging *GFO* with TP and *ERS-2* data first requires reduction of *GFO* orbit error and more generally removal of any inconsistency between *GFO*, TP, and *ERS-2* SSH. We followed the methodology proposed by Le Traon and Ogor (1998); TP, the most precise mission, is used as a reference for the other missions and *GFO* (*ERS-2*) orbit and long wavelength errors are removed through a global minimization of TP − GFO (TP − ERS-2) and GFO − GFO (ERS-2 − ERS-2) crossover differences (only crossovers with a time difference less than 10 days are used). The method proceeds as follows: each TP − GFO (TP − ERS-2) crossover difference gives an estimate of the *GFO* (*ERS-2*) orbit error with some noise. Smoothing cubic spline functions are then used to obtain a continuous estimation of orbit error over time. GFO − GFO (ERS-2 − ERS-2) crossovers further constrain the solution. After several sensitivity studies, we decided to use the same number and the same positions of spline knots as in Le Traon and Ogor (1998).

Statistics of crossover differences between the different missions before and after these crossover adjustments are given in Table 1. This shows that the methodology is very effective in reducing SSH inconsistencies between the different missions. *ERS-2* and *GFO* orbit errors, which are about 10 to 15 cm rms, are thus reduced to a level comparable to TP orbit error (about 2 cm rms). Note that the *GFO* crossover statistics after the adjustment are slightly better than *ERS-2* ones; this is probably because *GFO* has a smaller noise level than *ERS-2*.

c. Extracting sea level anomalies

When altimetric SSH data have been homogenized and intercalibrated, the next step is to extract the sea level anomalies for the different missions. This consists of removing a mean profile ⟨SSH⟩ from the individual SSH measurements (SLA = SSH − ⟨SSH⟩). The mean profile (MP) contains the geoid signal but also the mean

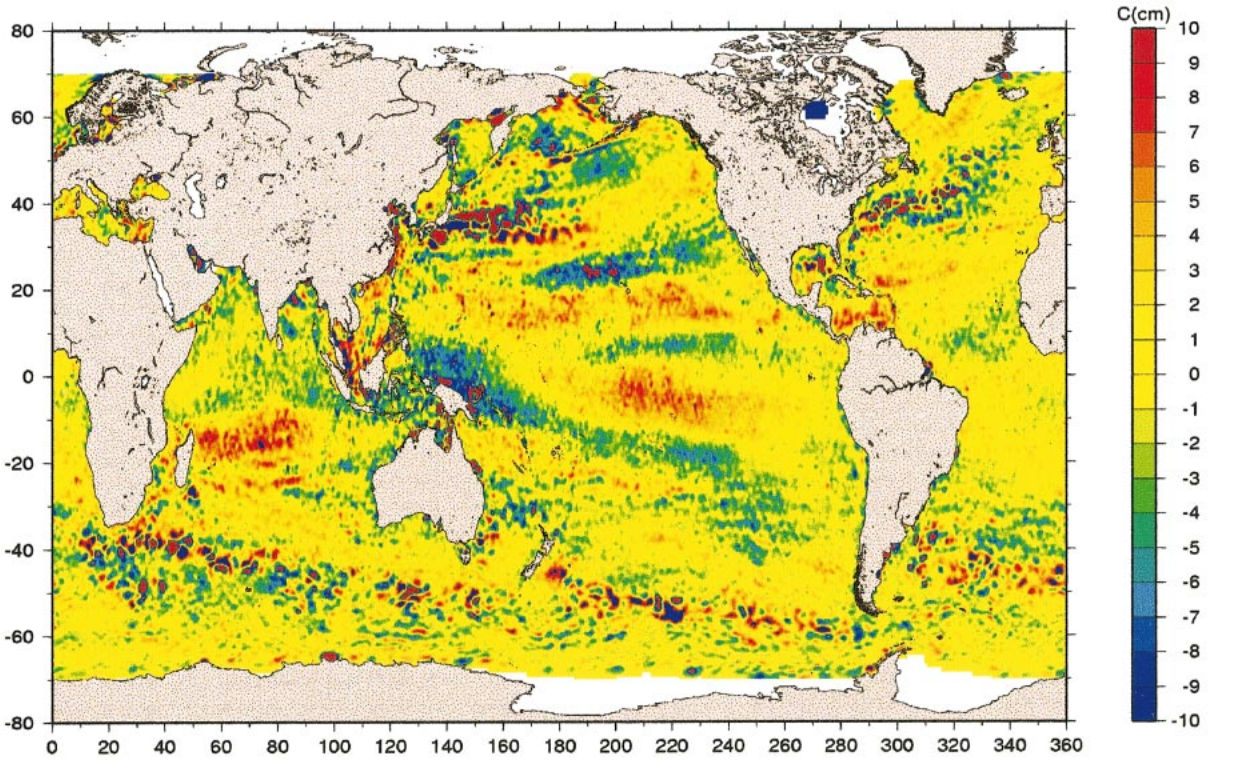

FIG. 1. Map of the TPG and EG crossover differences calculated using an objective analysis method.

dynamic topography (MDT) over the averaging period. We used for TP and *ERS-2* data MPs calculated over a 7-yr period (1993–99). The *ERS-2* mean profile uses both *ERS-1* and *ERS-2* data. A specific processing was applied to *ERS-1/2* data to get an MP consistent with TP. TOPEX/Poseidon data were thus used to correct *ERS-1/2* data both for orbit error and ocean variability. Because not enough *GFO* data are yet available, we used 2 yr of GEOSAT Exact Repeat Mission (ERM) data (1986–87; e.g., Douglas and Cheney 1990) to estimate an MP for *GFO*. As GEOSAT ERM and *GFO* have almost the same ground tracks, the geoid contained in the GEOSAT MP is consistent with the one measured by *GFO*. However, the GEOSAT MDT is not consistent with the TP and *ERS-2* MDT. The interannual sea level changes between the 1986–87 and the 1993–99 time periods could bias the *GFO* SLA relative to TP or *ERS-2* by several tens of centimeters (e.g., Fu and Chelton 2001). Moreover, SSHs measured by GEOSAT are much less accurate than the TP SSHs. The GEOSAT orbit is not determined better than the 10-cm level, and the wet tropospheric correction could not benefit from onboard radiometer measurements. All these effects induce mean SSH differences on a wide range of spatial scales, from a few tens of kilometers to systematic biases.

To reduce these errors, a procedure was applied to adjust the GEOSAT MP onto the TP and *ERS-2* MPs. A GEOSAT MP was first computed from the first 44 repeat cycles of the GEOSAT ERM (i.e., the 1986–87 period). The MP was then adjusted onto the TP and *ERS-2* MPs, using a least square fit of spline functions as in Le Traon and Ogor (1998). The spline minimization is constrained by TP − GEOSAT ($TP_{MP} - G_{MP}$) and GEOSAT − GEOSAT ($G_{MP} - G_{MP}$) MP crossover differences. ERS − GEOSAT ($E_{MP} - G_{MP}$) MP crossover differences were also used poleward of 66° to better constrain the estimation at high latitudes. This adjustment succeeded in reducing the GEOSAT MP errors at large scales (Table 2). Note that $TP_{MP} - G_{MP}$ and $E_{MP} - G_{MP}$ rms crossover differences are similar, which shows the good consistency of GEOSAT MP with the TP and *ERS-2* MPs.

However, the mapping of the $TP_{MP} - G_{MP}$ and $E_{MP} - G_{MP}$ crossover differences (Fig. 1) showed that discrepancies at shorter scales, located in high oceanic variability areas or in the Tropics, were not sufficiently reduced. These are mainly caused by ocean interannual variability or systematic biases like wet tropospheric or ionospheric errors in the equatorial band. These discrepancies exhibit a large zonally correlated pattern that can be removed. The $TP_{MP} - G_{MP}$ and $E_{MP} - G_{MP}$ crossover differences were thus mapped using an objective analysis to produce a medium-scale (scales larger than 200 km) correction field (see Fig. 1). This field was then removed to the GEOSAT MP. The correction does not improve, of course, the $G_{MP} - G_{MP}$ crossover differences as the same correction is applied to the ascending and descending tracks at a given crossover. The $E_{MP} - G_{MP}$

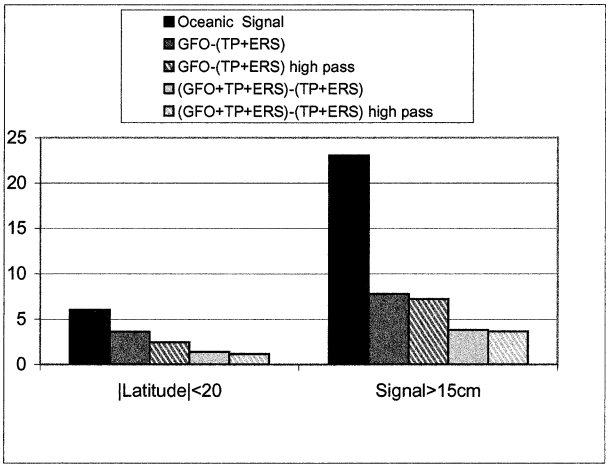

FIG. 2. Comparison of GFO and GFO + TP + ERS with TP + ERS maps in tropical regions and in regions where sea level variability is larger than 15 cm rms. Differences for wavelengths below 10° are also given. The rms of ocean signal is in black. Unit: cm.

and $TP_{MP} - G_{MP}$ crossover rms differences are, however, very significantly reduced down to a 3-cm level, yielding a GEOSAT MP that is much more consistent with the TP and *ERS-2* MPs.

As much less data are available, our *GFO* MP remains, of course, less accurate that the TP and *ERS-2* MPs (the rms of $TP_{MP} - TP_{MP}$, $E_{MP} - E_{MP}$, and $TP_{MP} - E_{MP}$ crossover differences are comprised between 1.5 and 2 cm). This will induce, however, only a small additional error (1–2 cm rms) in the SLA estimation.

d. Mapping technique

The final step is to merge the SLA data from the different altimeter missions via a mapping technique. We used the mapping method detailed in Le Traon et al. (1998) and applied to more than 5 yr of TP and *ERS-1/2* data by Ducet et al. (2000). This is a global suboptimal space–time objective analysis that takes into account along-track correlated errors. Several improvements were made compared to the version used by Ducet et al. (2000). In particular, we used an improved statistical description of sea level variability, noise, and long wavelength errors.

Covariance functions including propagation velocities that depend on geographical position were thus used. The correlation function $C(dx, dy, dt)$ has the following functional form:

$$C(r, t) = [1 + ar + 1/6(ar)^2 - 1/6(ar)^3] \times \exp(-ar)\exp(-t^2/T^2),$$

where

$$r = \sqrt{\left(\frac{dx - C_{px}dt}{L_x}\right)^2 + \left(\frac{dy - C_{py}dt}{L_y}\right)^2},$$

and dx, dy, and dt are the zonal/meridional space and time differences, and a is equal to 3.337.

For each grid point, the zonal and meridional spatial scales (first zero crossing of C) (L_x and L_y), the timescale T, and the zonal and meridional propagation velocities (C_{px} and C_{py}) were adjusted from 5 yr of TP + ERS-1/2 combined maps. As values are similar to the ones described in Jacobs et al. (2001), they will not be discussed here. The main differences with the values used by Ducet et al. (2000) come from the propagation velocities.

We used a white measurement noise of 3 cm for TP and 4 cm for *ERS-2* and *GFO* data. In addition, a noise of 10% of the signal variance was used to take into account the small scale variability, which cannot be mapped and should be filtered in the analysis (see discussion in Le Traon et al. 2001). Long wavelengths errors (LWEs) due to residual orbit errors but also tidal or inverse barometer errors and high-frequency ocean signals (e.g., Tierney et al. 2000) were also derived from an analysis of TP and *ERS-2* data. The relative variance of long wavelength errors varies between 1% and 2% in high-energy areas such as the Gulf Stream and can reach up to 40% in low-energy areas. For *GFO* LWE variance, we used the *ERS-2* values, but we also added a mean value of 25 cm^2. This ensures that *GFO* data will not modify the large-scale signals but will only contribute to the mesoscale variability mapping.

3. Results—Contribution of *GFO*

Global maps derived from *GFO* data alone and from the combination of TP and *ERS-2* (hereafter ERS) were first computed every 5 days from 15 December to 4 January (five maps) and compared. The difference between these two sets of maps should represent both sampling errors and measurement errors. As we expect that most of the measurement errors will result in large-scale errors, the difference maps were also high-pass filtered using a 2D Loess filter with a cutoff wavelength of 10°. This should allow us to quantify the contribution of sampling errors in the differences.

Figure 2 shows the rms of the GFO − (TP + ERS) differences for the total signal and for the high-pass signal in tropical/equatorial regions (20°S–20°N) and in regions dominated by mesoscale variability (sea level variability larger than 15 cm rms). In the latter, the differences are mainly at wavelengths below 10°. They are of about 15% of the signal variance and are consistent with the expected mapping errors of GFO and TP + ERS (e.g., Le Traon et al. 2001). They thus likely reflect the signals missed by *GFO* and TP + ERS. In the tropical/equatorial regions, the differences are larger (about 30% of the signal variance) and half of the variance of the differences is at large scales. The large-scale differences probably correspond to residual *GFO* orbit and ionospheric errors. Note, however, that the rms of the differences is of 3.5 cm rms. The *GFO* large-

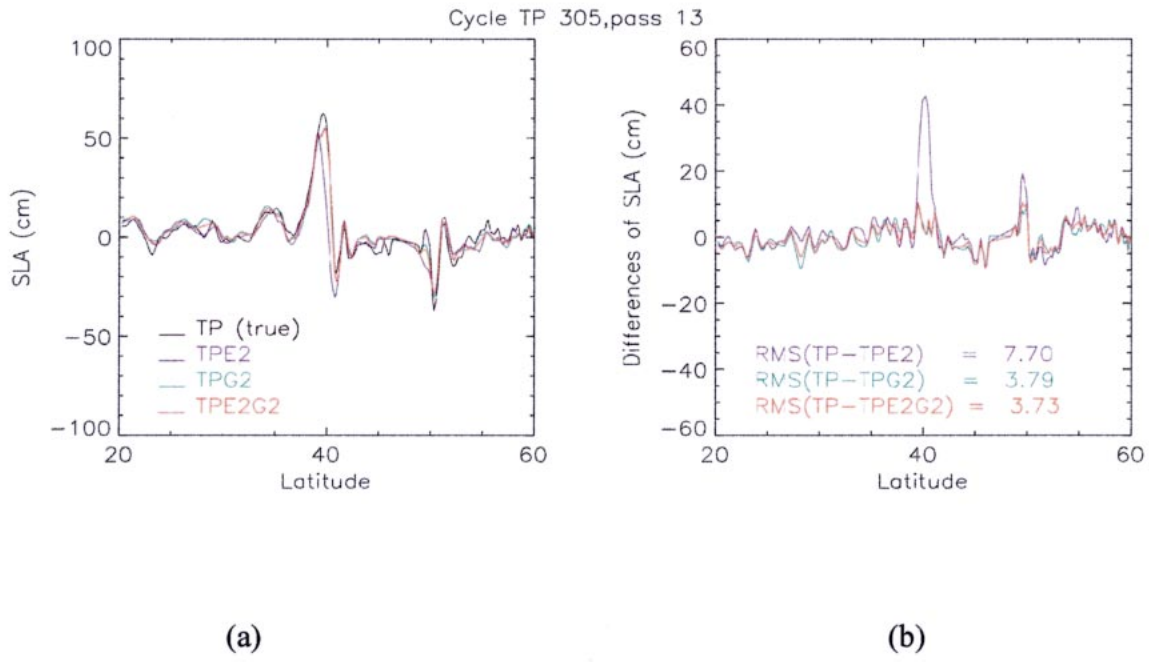

FIG. 3. Sea level anomaly estimated from the combination of TP, *ERS-2,* and *GFO* data along a TP track withheld from the mapping. Unit: cm.

scale errors (after the adjustment onto TP) are thus of a few centimeters rms only.

The next step was to combine *GFO* with TP and ERS. When *GFO* data are merged with TP + ERS-2 data, we expect that the *GFO* residual large-scale errors will not corrupt the combined maps because the mapping technique takes into account the long wavelength errors. GFO should only add information for the smaller scales and, in particular, the mesoscale signal. Figure 2 shows that the differences of the combined TP + ERS + GFO maps with the TP + ERS-2 maps are about 5% of the signal variance both in the tropical/equatorial regions and in the high variability areas. This is typically the mapping improvement that can be expected from the use of *GFO* data. The TP + ERS mean mapping error is, indeed, expected to be comprised of between 5% and 10% of the signal variance while the TP + ERS + GFO error should be smaller by a factor of about 1.5 (e.g., Le Traon et al. 2001). The rms of the difference between the five TP + ERS + GFO and TP + ERS maps (not shown) confirms that the differences are mostly found in large eddy variability regions (where they can be larger than 7 cm rms), while in low eddy energy regions the differences are often smaller than 1 cm rms.

The difference between the TP + ERS + GFO and TP + ERS maps does not prove, however, that the additional use of *GFO* provides an improved description. To better quantify the contribution of the combination, a few TP tracks were removed from the TP SLA dataset to serve as a reference. We then analyzed how well we can reconstruct the sea level variations under these tracks using TP + ERS and TP + ERS + GFO data. In areas with a large sea level variability (>15 cm rms) the rms of the differences is 10.16 with TP + ERS and 8.00 with TP + ERS + GFO. This shows that GFO allows a reduction of the mapping error variance by a factor of 1.6. This is a very significant improvement. It is consistent with our formal mapping errors. Figure 3 is an example of a TP track for which the use of *GFO* has provided a much better estimation of the sea level variations near the Gulf Stream area. The TP + ERS combination misplaced an eddy near the Gulf Stream, which induced a mapping error of about 40 cm. Since *GFO* data were available close to this position, the signal was captured by the combination of TP, ERS, and *GFO* data and the mapping error largely reduced.

Finally, Fig. 4 illustrates the contribution of *GFO* in the Gulf Stream region. Two maps of sea level anomaly derived from, respectively, TP + ERS and TP + ERS + GFO and their difference are shown. Differences are localized close to the *GFO* tracks, which are adding information only when the estimation is not constrained enough by TP and ERS. In general structures from the TP + ERS + GFO map are more intense because signals are better resolved. There is, in particular, a cold eddy near 39.5°N, 304°E associated with a meander of the Gulf Stream that is better represented in the TP + ERS + GFO map (differences with the TP + ERS map here are larger than 20 cm).

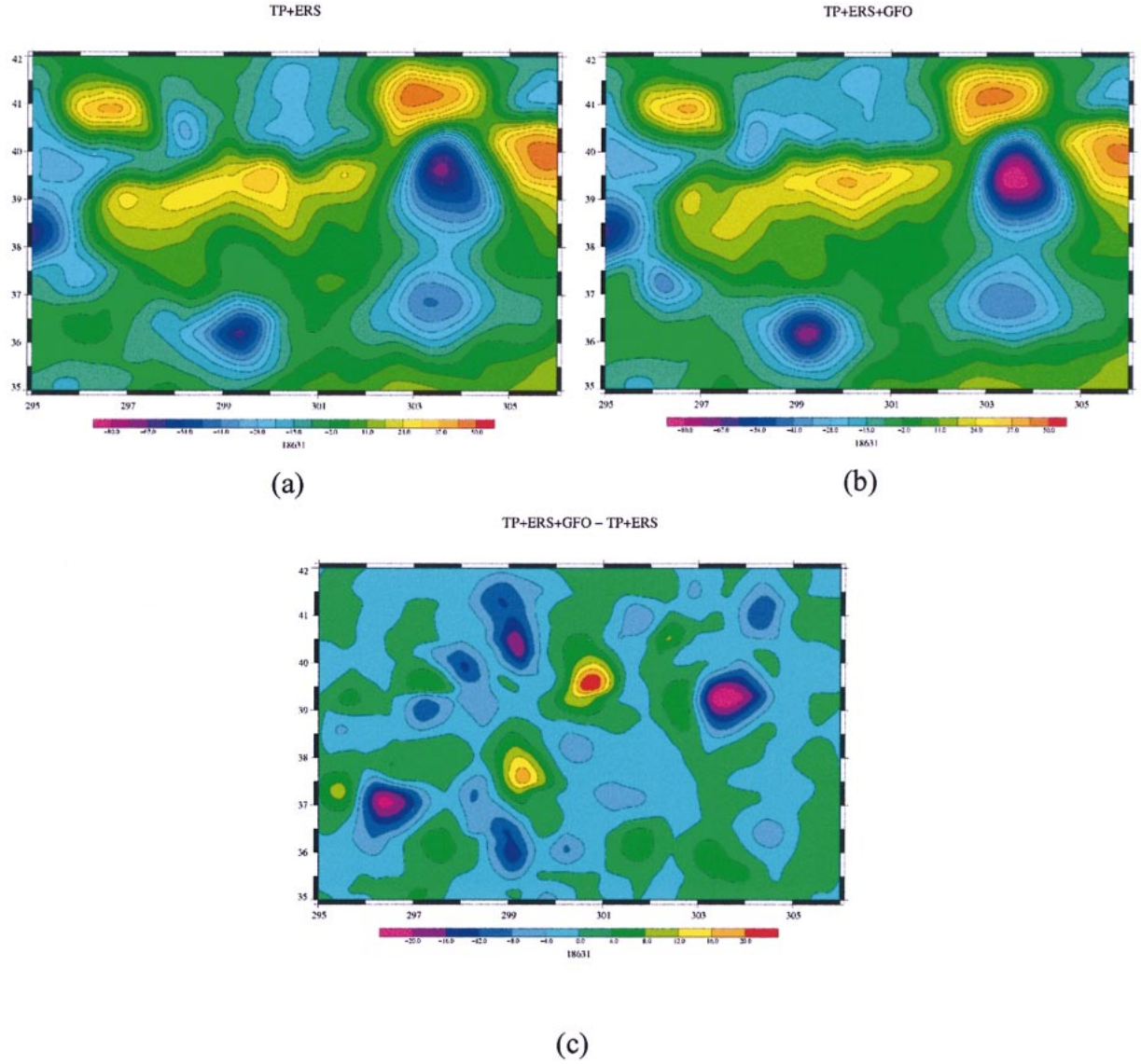

FIG. 4. Sea level anomaly maps derived from the merging of (a) TP + ERS-2 and (b) TP + ERS-2 + GFO in the Gulf Stream region on 4 Jan 2001. The difference between (a) and (b) is given in (c). Unit: cm.

4. Conclusions/perspectives

Effective techniques to merge *GFO* with TP and *ERS-2* data have been developed. Thanks to these techniques, we have shown that *GFO* can be combined with TP and *ERS-2* and that the combination provides a significant improvement in the description of the mesoscale ocean circulation. The study will now be extended to a larger *GFO* dataset to better quantify the contribution of *GFO* data. The merging techniques and *GFO* data will also soon be implemented in the SSALTO/DUACS near-real-time multiple altimeter processing system to serve operational oceanography projects, and, in particular, the Global Ocean Data Assimilation Experiment (GODAE).

Acknowledgments. We thank J. Lillibridge for providing us with the NOAA *GFO* data and for useful comments on an earlier version of this paper. This study was supported by CNES under Contract 731/CNES/00/8435/00-CLS and SHOM under Contract No. 01.87.044.00.470.29.25.

REFERENCES

Douglas, B. C., and R. E. Cheney, 1990: GEOSAT: Beginning a new era in satellite oceanography. *J. Geophys. Res.*, **95,** 2833–2836.

Ducet, N., P.-Y. Le Traon, and G. Reverdin, 2000: Global high resolution mapping of ocean circulation from TOPEX/POSEIDON and *ERS-1* and *-2. J. Geophys. Res.*, **105,** 19 477–19 498.

Fu, L.-L., and D. Chelton, 2001: Large-scale ocean circulation. *Sat-*

ellite Altimetry and Earth Sciences. A Handbook of Techniques and Applications, L.-L. Fu and A. Cazenave, Eds., Academic Press, 133–169.

International GODAE Steering Team, 2001: The Global Ocean Data Assimilation Experiment: Strategic plan. GODAE Rep. 6, Melbourne, Australia, 6 pp.

Jacobs, G. A., C. N. Barron, and R. C. Rhodes, 2001: Mesoscale characteristics. *J. Geophys. Res.,* **106,** 19 581–19 595.

Koblinsky, C. J., P. Gaspar, and G. Lagerloef, Eds., 1992: *The Future of Spaceborne Altimetry: Oceans and Climate Change.* Joint Oceanographic Institutions Incorporated, 75 pp.

Le Traon, P.-Y., and F. Ogor, 1998: *ERS-1/2* orbit improvement using TOPEX/POSEIDON: The 2 cm challenge. *J. Geophys. Res.,* **103,** 8045–8057.

——, and R. A. Morrow, 2001: Ocean currents and mesoscale eddies. *Satellite Altimetry and Earth Sciences. A Handbook of Techniques and Applications*, L.-L. Fu and A. Cazenave, Eds., Academic Press, 171–215.

——, F. Nadal, and N. Ducet, 1998: An improved mapping method of multisatellite altimeter data. *J. Atmos. Oceanic Technol.,* **15,** 522–534.

——, G. Dibarboure, and N. Ducet, 2001: Use of a high-resolution model to analyze the mapping capabilities of multiple-altimeter missions. *J. Atmos. Oceanic Technol.,* **18,** 1277–1288.

Picaut, J., and A. J. Busalacchi, 2001: Tropical ocean variability. *Satellite Altimetry and Earth Sciences. A Handbook of Techniques and Applications*, L.-L. Fu and A. Cazenave, Eds., Academic Press, 217–236.

Ray, R., 1999: A global ocean tide model from TOPEX/Poseidon altimetry: GOT99.2. NASA Tech. Memo. NASA/TM-1999-209478, 58 pp.

Scharroo, R., and P. Visser, 1998: Precise orbit determination and gravity field improvement for the ERS satellites. *J. Geophys. Res.,* **103,** 8113–8127.

Tierney, C., J. Wahr, F. O. Bryan, and V. Zlotnicki, 2000: Short-period oceanic circulation: Implications for satellite altimetry. *Geophys. Res. Lett.,* **27,** 1255–1258.